

# Simulation studies of $R_2(\Delta\eta, \Delta\varphi)$ and $P_2(\Delta\eta, \Delta\varphi)$ correlation functions in pp collisions with the PYTHIA and HERWIG models

Baidyanath Sahoo,<sup>1,\*</sup> Basanta Kumar Nandi,<sup>1</sup> Prabhat Pujahari,<sup>2</sup> Sumit Basu,<sup>3,†</sup> and Claude Pruneau<sup>3,‡</sup>

<sup>1</sup>*Department of Physics, Indian Institute of Technology Bombay, Mumbai - 400076, India*

<sup>2</sup>*Department of Physics, Indian Institute of Technology Madras, Chennai - 600025, India*

<sup>3</sup>*Department of Physics and Astronomy, Wayne State University, Detroit, 48201 USA*

(Dated: November 26, 2021)

We report studies of charge-independent (CI) and charge-dependent (CD) two-particle differential-number correlation functions,  $R_2(\Delta\eta, \Delta\varphi)$ , and transverse momentum ( $p_T$ ) correlation functions,  $P_2(\Delta\eta, \Delta\varphi)$ , of charged particles in  $\sqrt{s} = 2.76$  TeV pp collisions with the PYTHIA and HERWIG models. Model predictions are presented for inclusive charged hadrons ( $h^\pm$ ), as well as pions ( $\pi^\pm$ ), kaons ( $K^\pm$ ), and (anti-)protons ( $\bar{p}/p$ ) in the ranges  $0.2 < p_T \leq 2.0$  GeV/ $c$ ,  $2.0 < p_T \leq 5.0$  GeV/ $c$ , and  $5.0 < p_T \leq 30.0$  GeV/ $c$ , with full azimuthal coverage in the range  $|\eta| < 1.0$ . We compare the model predictions for the strength and shape of the  $R_2$  and  $P_2$  correlators as these pertain to recent measurements by the ALICE collaboration. The  $R_2$  and  $P_2$  correlation functions estimated with PYTHIA and HERWIG exhibit qualitatively similar near-side and away-side correlation structures but feature important differences. Our analysis indicates that comparative studies of  $R_2$  and  $P_2$  correlation functions would provide valuable insight towards the understanding of particle production in pp collisions, and by extension, should also be useful in studies of heavy-ion collisions. Comparison of the  $\Delta\eta$  dependence of  $R_2$  and  $P_2$  could contribute, in particular, to a better understanding and modeling of the angular ordering of particles produced by hadronization in jets, as well as a better description of jet fragmentation functions of identified species at low momentum fraction ( $z$ ).

PACS numbers: 25.75.Gz, 25.75.Ld, 24.60.Ky, 24.60.-k

arXiv:1810.09747v2 [nucl-ex] 27 Aug 2019

---

\* baidya@iitb.ac.in

† sumit.basu@cern.ch

‡ claude.pruneau@wayne.edu

## I. INTRODUCTION

Measurements of integral and differential correlation functions constitute essential tools for the study of proton-proton (pp) and heavy-ion (A–A) collisions at relativistic energies. Two- and multi-particle azimuthal correlations functions have provided evidence for the existence of anisotropic flow in A–A collisions [1–7], quark scaling (approximate) of flow coefficients in A–A collisions at RHIC and LHC [8–11]. They were also used to investigate the presence of flow in smaller systems (e.g., p–A and high multiplicity pp collisions) [12–17]. Differential two-particle (number) correlation functions additionally enabled the discovery of jet quenching at RHIC [18, 19] and its detailed characterization in A–A collisions at both RHIC and LHC [20]. Several other correlation functions, including number and transverse momentum correlation functions [21, 22] have been measured and investigated both at RHIC and LHC to better understand the particle production dynamics and study the properties of the matter produced in pp and A–A collisions [23–28]. Among these, the recent measurements of number correlation,  $R_2$ , and differential transverse momentum correlation,  $P_2$ , defined in Sec. II, have enabled independent confirmation of the collective nature of the azimuthal correlations observed in Pb–Pb collisions [29], as well as the identification of noticeable differences in the  $\Delta\eta$  and  $\Delta\varphi$  dependence of these correlation functions [28]. These measurements show that the near-side peak of both CI and CD correlations is significantly narrower, at any given A–A collision centrality in  $P_2$  than in  $R_2$  correlation functions. This confirms [30] that comparative measurements of  $P_2$  and  $R_2$  correlation functions may provide additional sensitivity to the underlying particle production mechanisms in heavy-ion collisions. In this work, we seek to establish whether the difference observed in [28] can be readily explained by jet contributions. To this end, we examine predictions of the  $R_2$  and  $P_2$  correlation functions by the PYTHIA [31] and HERWIG [32] models that are known to quantitatively reproduce many jet related observables reported and compiled by RHIC and LHC experiments [33–35]. We examine the differential correlation functions  $R_2$  and  $P_2$  in pp collisions with a particular focus on particles produced in the range  $0.2 < p_T \leq 2.0$  GeV/ $c$  reported by ALICE [28, 29] but also extend our study to include higher momentum ranges to further examine how the two observables behave for higher particle momenta expected to be dominated by jet production.

Particle production in high-energy nucleus-nucleus collisions is governed by several conservation laws including (electric) charge conservation, baryon number conservation, strangeness conservation, as well as energy-momentum conservation. At very large collision energy, the yield of anti-particles and particles are nearly equal. Limited information is thus gained by studying the yields, e.g.,  $\pi^+$  and  $\pi^-$  individually. Additional insight may be provided, however, by comparative studies of like-sign (LS) and unlike-sign (US) particle pairs, e.g.,  $\pi^+, \pi^+$  and  $\pi^+, \pi^-$ , or baryon-baryon and baryon-anti-baryon particle pairs. We thus study predictions of the models for both charge-independent (CI) and charge-dependent (CD) pair combinations.

This paper is organized as follows. Section II presents definitions of the  $R_2$  and  $P_2$  correlation functions studied in this work and describes how they are computed. The PYTHIA and HERWIG models, and the conditions under which they were used to generate pp events, are briefly described in Sec. III. Predictions by the models for  $R_2$  and  $P_2$  correlation functions are presented in Sec. IV and conclusions are summarized in Sec. V.

## II. CORRELATION FUNCTIONS DEFINITION

The  $R_2$  and  $P_2$  correlation functions are defined in terms of single- and two-particle densities expressed as functions of the particle pseudo-rapidity  $\eta$  and azimuthal angle  $\varphi$

$$\rho_1(\eta, \varphi) = \frac{1}{\sigma_1} \frac{d^2\sigma_1}{d\eta d\varphi}, \quad (1)$$

$$\rho_2(\eta_1, \varphi_1, \eta_2, \varphi_2) = \frac{1}{\sigma_2} \frac{d^4\sigma_2}{d\eta_1 d\varphi_1 d\eta_2 d\varphi_2}, \quad (2)$$

where  $\sigma_1$  and  $\sigma_2$  are single and two-particle cross-sections, respectively. The correlator  $R_2$  is defined as a two-particle cumulant normalized by the product of single-particle densities (hereafter called normalized

two-particle cumulant) according to

$$R_2(\eta_1, \varphi_1, \eta_2, \varphi_2) = \frac{\rho_2(\eta_1, \varphi_1, \eta_2, \varphi_2)}{\rho_1(\eta_1, \varphi_1)\rho_1(\eta_2, \varphi_2)} - 1, \quad (3)$$

while the  $P_2$  correlation function is defined in terms of the differential correlator  $\langle \Delta p_T \Delta p_T \rangle$  normalized by the square of the average transverse momentum,  $p_T$ , to make it dimensionless, as follows

$$P_2(\eta_1, \varphi_1, \eta_2, \varphi_2) = \frac{\langle \Delta p_T \Delta p_T \rangle(\eta_1, \varphi_1, \eta_2, \varphi_2)}{\langle p_T \rangle^2}. \quad (4)$$

The  $\langle \Delta p_T \Delta p_T \rangle$  differential correlator [30] is defined according to

$$\langle \Delta p_T \Delta p_T \rangle(\eta_1, \varphi_1, \eta_2, \varphi_2) = \frac{\int_{p_{T,\min}}^{p_{T,\max}} \Delta p_{T,1} \Delta p_{T,2} \rho_2(\vec{p}_1, \vec{p}_2) dp_{T,1} dp_{T,2}}{\int_{p_{T,\min}}^{p_{T,\max}} \rho_2(\vec{p}_1, \vec{p}_2) dp_{T,1} dp_{T,2}} \quad (5)$$

where  $\Delta p_{T,i} = p_{T,i} - \langle p_T \rangle$  and  $\langle p_T \rangle$  is the inclusive mean transverse momentum

$$\langle p_T \rangle = \frac{\int_{p_{T,\min}}^{p_{T,\max}} \rho_1 p_T dp_T}{\int_{p_{T,\min}}^{p_{T,\max}} \rho_1 dp_T}. \quad (6)$$

In addition to its sensitivity to the presence of particle correlations,  $P_2$  is also determined by the momentum of the correlated particles [29]. It is positive whenever particle pairs emitted at specific azimuthal angle and pseudo-rapidity differences are more likely to both have transverse momenta higher (or lower) than the  $\langle p_T \rangle$  and negative when a high- $p_T$  particle ( $p_T > \langle p_T \rangle$ ) is more likely to be accompanied by a low- $p_T$  particle ( $p_T < \langle p_T \rangle$ ). For instance, particles emitted within a jet typically have higher  $p_T$  than the inclusive average. Jets, therefore, contribute a large positive value to  $P_2$ . Hanbury-Brown and Twiss (HBT) correlations, determined by pairs of identical particles with  $p_{T,1} \approx p_{T,2}$  should likewise contribute positively to this correlator. However, particle production involving a mix of low- and high-momenta correlated particles can contribute both positively and negatively. Based on this simple observation, one expects the internal structure of jets to influence the  $\Delta\eta$ ,  $\Delta\varphi$  dependence of the near-side peak of  $P_2$  correlation functions. Within jets, as schematically illustrated in Fig. 1, high- $p_T$  particles are predominantly

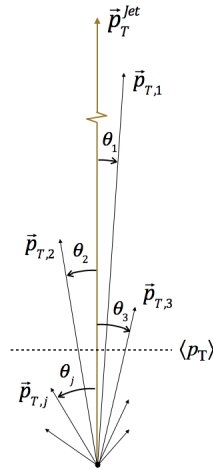


FIG. 1. Schematic representation of the transverse momentum and angular ordering of jet constituents relative to the jet axis,  $\vec{p}_T^{jet}$ .

emitted at small polar angles relative to the jet axis, while lower  $p_T$  particles span a larger angular range.

This leads to an effective ordering of the particles (typical)  $p_T$  relative to the polar angle  $\theta$ . In turn, this also leads to an effective  $p_T$  ordering in the  $\Delta\eta$  vs.  $\Delta\varphi$  plane. For instance, one expects that for small  $\Delta\eta$ ,  $\Delta\varphi$  separations, high- $p_T$  particles (i.e.,  $p_{T,i} \gg \langle p_T \rangle$ ) should dominate the  $P_2$  correlation and contribute positive  $\Delta p_T \Delta p_T$  values. Likewise, at very large  $\Delta\eta$ ,  $\Delta\varphi$  separation, the correlation strength should be determined by particle pairs with  $p_{T,i} < \langle p_T \rangle$  thereby also yielding positive  $\Delta p_T \Delta p_T$  values. However, there shall also be an intermediate  $\Delta\eta$ ,  $\Delta\varphi$  range such that pairs consist of one high- $p_T$  particle and one low- $p_T$  particle yielding negative  $\Delta p_T \Delta p_T$  values on average. This should thus produce a narrowing and possibly a non-monotonic  $\Delta\eta$ ,  $\Delta\varphi$  dependence of the correlation strength. We shall demonstrate, in the following, that both PYTHIA and HERWIG do in fact exhibit such behavior.

In this work, the correlators  $R_2$  and  $P_2$  are reported as function of the differences  $\Delta\eta = \eta_1 - \eta_2$  and  $\Delta\varphi = \varphi_1 - \varphi_2$  by averaging across the mean pseudo-rapidity  $\bar{\eta} = \frac{1}{2}(\eta_1 + \eta_2)$  and the mean azimuthal angle  $\bar{\varphi} = \frac{1}{2}(\varphi_1 + \varphi_2)$  acceptance according to

$$O(\Delta\eta, \Delta\varphi) = \frac{1}{\Omega(\Delta\eta)} \int O(\eta_1, \varphi_1, \eta_2, \varphi_2) \delta(\Delta\varphi - \varphi_1 + \varphi_2) d\varphi_1 d\varphi_2 \times \delta(\Delta\eta - \eta_1 + \eta_2) d\eta_1 d\eta_2, \quad (7)$$

where  $\Omega(\Delta\eta)$  represents the width of the acceptance in  $\bar{\eta}$  at a given value of  $\Delta\eta$  and angle differences  $\Delta\varphi$  are calculated modulo  $2\pi$  and shifted by  $-\pi/2$  for convenience of representation in the figures. The analysis of the  $R_2$  and  $P_2$  correlation functions are carried out for charge combination pairs  $(+-)$ ,  $(-+)$ ,  $(++)$ , and  $(--)$  separately. Like-sign pairs correlations are averaged to yield LS correlations,  $O^{\text{LS}} = \frac{1}{2}[O^{++} + O^{--}]$ , and US correlators are obtained by averaging  $(+-)$  and  $(-+)$  correlations,  $O^{\text{US}} = \frac{1}{2}[O^{+-} + O^{-+}]$ . The LS and US correlations are then combined to yield charge-independent and charge-dependent correlation functions according to

$$O^{\text{CI}} = \frac{1}{2} [O^{\text{US}} + O^{\text{LS}}], \quad (8)$$

$$O^{\text{CD}} = \frac{1}{2} [O^{\text{US}} - O^{\text{LS}}]. \quad (9)$$

The CI correlation function measures the average of all correlations between charged particles while the CD correlation function is sensitive to the difference of US and LS pairs and is largely driven, as such, by charge conservation effects. The CD correlation function is proportional to the charge balance function [23] when the yields of positive and negative particles are equal [36].

We repeated the analysis and used the sub-sampling technique to obtain a more accurate estimation of statistical uncertainty. The Monte Carlo data sample was divided into 10 segments of equal size—e.g. equal number of events. Each sub-sample was analyzed independently. We then extracted the mean values and calculated the sample standard deviations ( $\sigma$ ) according to

$$\sigma = \sqrt{\frac{\sum_i (O_i - \langle O \rangle)^2}{N - 1}} \quad (10)$$

where “N-1” used instead of “N” depending on Bessel’s correction and , where  $i=1,2,\dots,10$ . The error on the mean is calculated bin-by-bin using the general formula  $\sigma_{\text{error}} = \frac{\sigma}{\sqrt{N}}$  .

### III. MONTE CARLO MODELS

The impact of jet production on  $R_2$  and  $P_2$  correlation functions in pp is studied with Monte Carlo simulations carried out with the event generators PYTHIA 6.425, tune Perugia-0 [31, 37–40], and HERWIG 6.5 [32]. PYTHIA and HERWIG are both based on QCD at Leading Order (LO) but use different parton production and hadronization schemes. PYTHIA uses the Lund string fragmentation model for high- $p_T$  parton hadronization while the production of soft particles (i.e., the underlying event) is handled through fragmentation of mini-jets from initial and final state radiation, multiple parton interactions (MPI),

and proton remnants [41]. The kPyJets process responsible for jet production uses the CTEQ6l [42] parametrization of the proton parton distribution function (PDF) tuned for LHC energies. HERWIG events were generated based on the jet generation process 1500 [32] and the CTEQ5L [43] parametrization of the proton PDFs with hard color-singlet exchange between two partons [44] using leading-logarithmic (LL) BFKL [45] calculations in ALICE environment. In HERWIG, the perturbative parton evolution ends with the production of clusters subsequently decayed into final-state hadrons.

In order to study the correlation functions with reliable statistical accuracy, and given the jet production cross-section falls steeply with increasing transverse momentum, we generated equal number of PYTHIA and HERWIG events in three hard QCD ( $2 \rightarrow 2$  processes)  $p_T$  bins: 5.0 - 10.0 GeV/ $c$ , 10.0 - 20.0 GeV/ $c$ , and 20.0 - 30.0 GeV/ $c$  [46]. A total of  $2 \times 10^8$  events were generated with PYTHIA and  $2 \times 10^8$  HERWIG events were produced in each  $\hat{p}_T$  bins. Single- and two-particle densities were calculated independently in each  $\hat{p}_T$  bin and averaged with weights corresponding to their respective fractional cross-sections.

Charge, baryon number, or strangeness balance function [23] are of interest to study the role of conservation laws and the dynamics of particle transport in elementary and heavy-ion collisions. However, charge balance functions should be proportional and thus equivalent to the correlator  $R_2^{CD}$  provided the measured multiplicities of positively and negatively charged particles are equal. We verified the applicability of the equivalence by comparing the differential cross-sections of positively and negatively charged hadrons,  $h^\pm$ , and found that the ratio of cross-sections is of order unity in the  $p_T$  range of interest of this study. It is then legitimate to use the  $R_2^{CD}$  correlation function as a proxy for the balance function: balance functions are thus not explicitly reported in this study.

#### IV. MODEL PREDICTIONS

We begin with a discussion of unidentified charged hadron correlation functions in sec. IV A. Correlation functions for identified particles, e.g., pions, kaons, and protons, are presented in sec. IV C.

##### A. Inclusive charged hadron correlations

We focus our discussion on CI and CD correlation functions. Associated balance functions,  $B$ , can be obtained by multiplying  $R_2^{CD}$  correlation functions with integrals of the hadron cross-sections. Figure 2 illustrates the calculation of CI and CD correlation functions based on the correlators  $R_2^{US}$  and  $R_2^{LS}$ . Panels (a,b) present examples of these correlation functions calculated with PYTHIA for particles in the transverse momentum range  $0.2 < p_T \leq 2.0$  GeV/ $c$  and pseudo-rapidity range  $|\eta| < 1.0$ . The US and LS correlation functions are combined according to Eqs. (8) and (9) to obtain CI and CD correlation functions shown in panels (c,d) of the same figure.

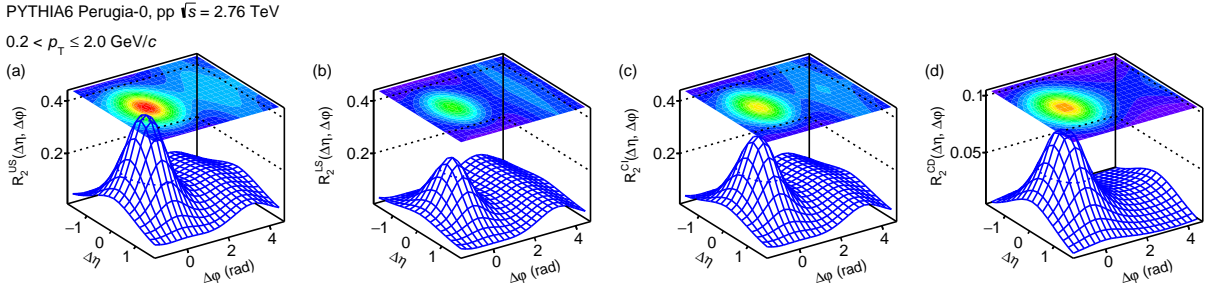


FIG. 2. Normalized two-particle cumulants (a)  $R_2^{US}$ , (b)  $R_2^{LS}$ , (c)  $R_2^{CI}$ , (d)  $R_2^{CD}$  obtained from PYTHIA simulations of pp collisions at  $\sqrt{s} = 2.76$  TeV for charged hadrons in the pseudo-rapidity range  $|\eta| < 1.0$  and the transverse momentum range  $0.2 < p_T \leq 2.0$  GeV/ $c$ .

The US and LS correlation functions both feature a prominent near-side peak centered at  $(\Delta\eta, \Delta\phi) =$

(0, 0). One notes, however, that the peak observed in US correlation functions is taller than that observed in LS correlation functions. This leads to a modest and narrow near-side peak in the CD correlation function shown in panel (d). The amplitude and shape of this peak are determined by the (charge) pair production and hadronization processes. We show in this article that PYTHIA and HERWIG make quantitatively different predictions of these features. Measurements of  $R_2^{\text{CD}}$  correlation functions shall thus provide a valuable basis to test the underlying mechanisms used in these models for  $q\bar{q}$  pair creation and hadronization of partons into hadrons,  $q(\bar{q}) \rightarrow h^\pm$ .

### 1. Charge Independent Correlations

We first compare the  $R_2$  and  $P_2$  correlation functions for CI charge combinations obtained in simulations of pp collisions with the PYTHIA and HERWIG generators. Figures 3 and 4 present the  $R_2^{\text{CI}}$  and  $P_2^{\text{CI}}$  correlation functions, respectively.

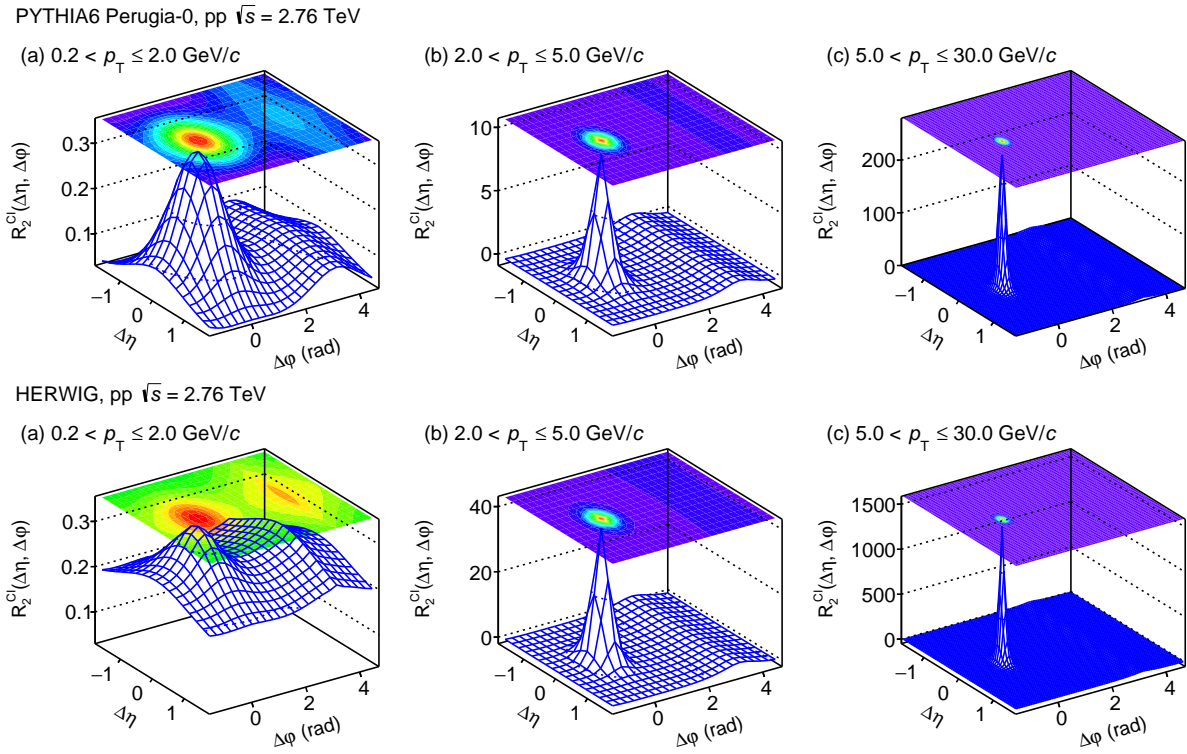


FIG. 3. Correlation functions  $R_2^{\text{CI}}$  of charged hadrons, in selected  $p_T$  ranges, obtained with PYTHIA (top panel) and HERWIG (bottom panel) in pp collisions at  $\sqrt{s} = 2.76$  TeV.

Correlation functions are presented for unidentified charged hadrons calculated in momentum ranges: (i)  $0.2 < p_T \leq 2.0$  GeV/c, (ii)  $2.0 < p_T \leq 5.0$  GeV/c, and (iii)  $5.0 < p_T \leq 30.0$  GeV/c. In these and the following figures, the  $\langle p_T \rangle$  values used for the calculation of  $\Delta p_T \Delta p_T$  are the  $p_T$  averages of particles produced in each of these three ranges, respectively. The first momentum range samples the underlying event in pp collisions and is relevant for comparisons with bulk particle production in A–A collisions. The second range corresponds to the coalescence range [47, 48], while the third range shifts the focus on particles produced by jet fragmentation. We find calculations of the  $R_2$  and  $P_2$  correlation functions in these three ranges yield qualitatively similar results. However, they also exhibit interesting quantitative differences which we discuss in details, in the following, based on projections onto the  $\Delta\eta$

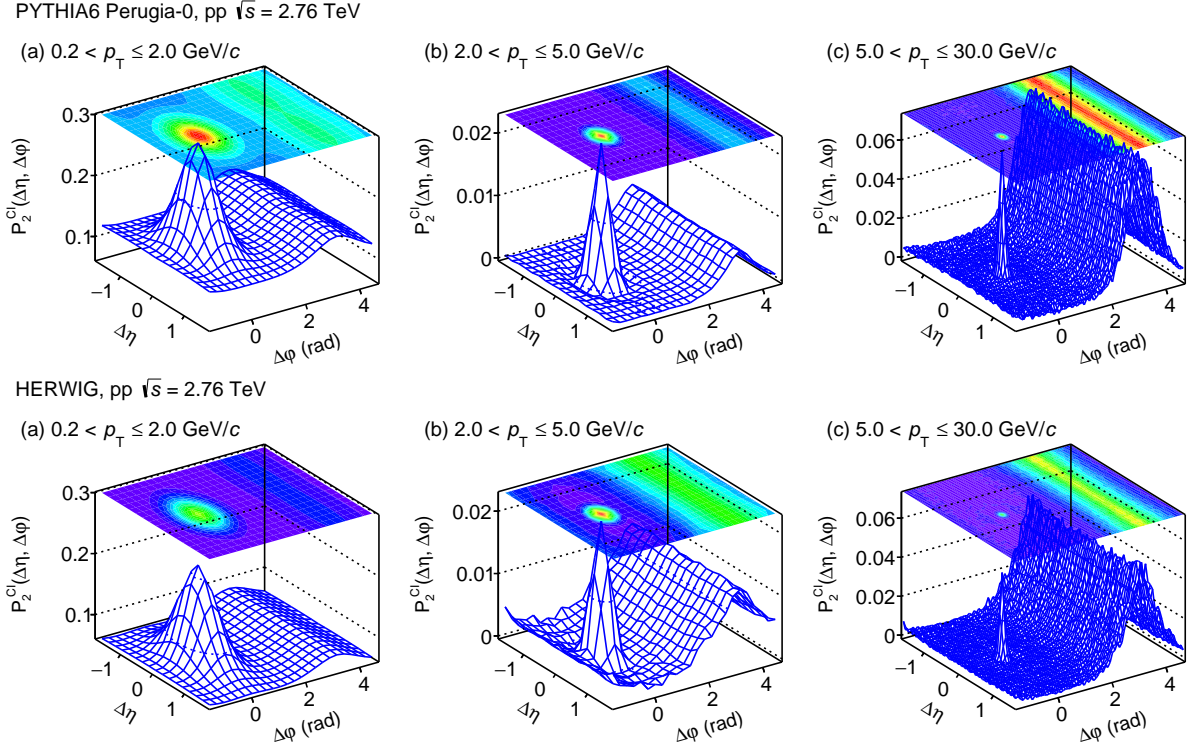


FIG. 4. Correlation functions  $P_2^{CI}$  of charged hadrons, in selected  $p_T$  ranges, obtained with PYTHIA (top panel) and HERWIG (bottom panel) in pp collisions at  $\sqrt{s} = 2.76$  TeV.

and  $\Delta\phi$  axes. The  $R_2^{CI}$  and  $P_2^{CI}$  correlation functions feature a prominent near-side peak centered at  $(\Delta\eta, \Delta\phi) = (0, 0)$  as well as an away-side structure, centered at  $\Delta\phi = \pi$ , and extending across the range  $|\Delta\eta| \leq 1.6$  (truncated in the figure to avoid the fluctuations at larger  $\Delta\eta$ ). Such near-side and away-side features have been observed in triggered and non-triggered correlation function measured in a variety of collision systems and beam energies [14, 19, 28, 29, 49–51]. In this work, we study the predictions of the PYTHIA and HERWIG models relative to their dependence on the particle momenta, the particle species, and we focus, in particular, on the differences between  $R_2$  and  $P_2$  correlation functions.

In Figs. 3 and 4, one observes the longitudinal and azimuthal widths of the near-side peak of the  $R_2^{CI}$  and  $P_2^{CI}$  correlation functions predicted by the two models decrease monotonically with the  $p_T$  range of the particles. Additionally, the near-side peak of  $P_2^{CI}$  correlations are systematically narrower than those observed in the  $R_2^{CI}$  correlation functions, as reported by the ALICE collaboration [28, 29]. These differences are studied quantitatively based on the projections of the correlation functions onto the  $\Delta\eta$  and  $\Delta\phi$  axes presented in Figs. 5 and 6.

Projections of the  $R_2^{CI}$  and  $P_2^{CI}$  correlation functions onto the  $\Delta\eta$  axis calculated with the PYTHIA and HERWIG models are presented in the left and right panels of Fig. 5, respectively, for the three  $p_T$  ranges already considered. One observes that the models make quantitatively different predictions for both correlation functions in all three  $p_T$  ranges. Indeed, both models yield peaks centered at  $(\Delta\eta, \Delta\phi) = (0, 0)$  but the shape and strength of these peaks differ markedly across models. The strengths and widths of the peaks also evolve differently with  $p_T$ . One notes, additionally, that the calculations for  $P_2^{CI}$  exhibit quite noticeable differences with  $R_2^{CI}$ : they feature narrower peaks and different ordering in the strengths predicted by the models. The RMS widths of these projections are plotted in Fig. 12 and discussed in more details in sec. IV B. It is clear at the outset, however, that measurements of both  $R_2^{CI}$  and  $P_2^{CI}$  in pp collisions with different  $p_T$  ranges should in principle provide significant constraints on the models and their underlying particle production mechanisms.

Caution in the interpretation of the widths of the near-side peak of the  $P_2^{CI}$  correlation functions is

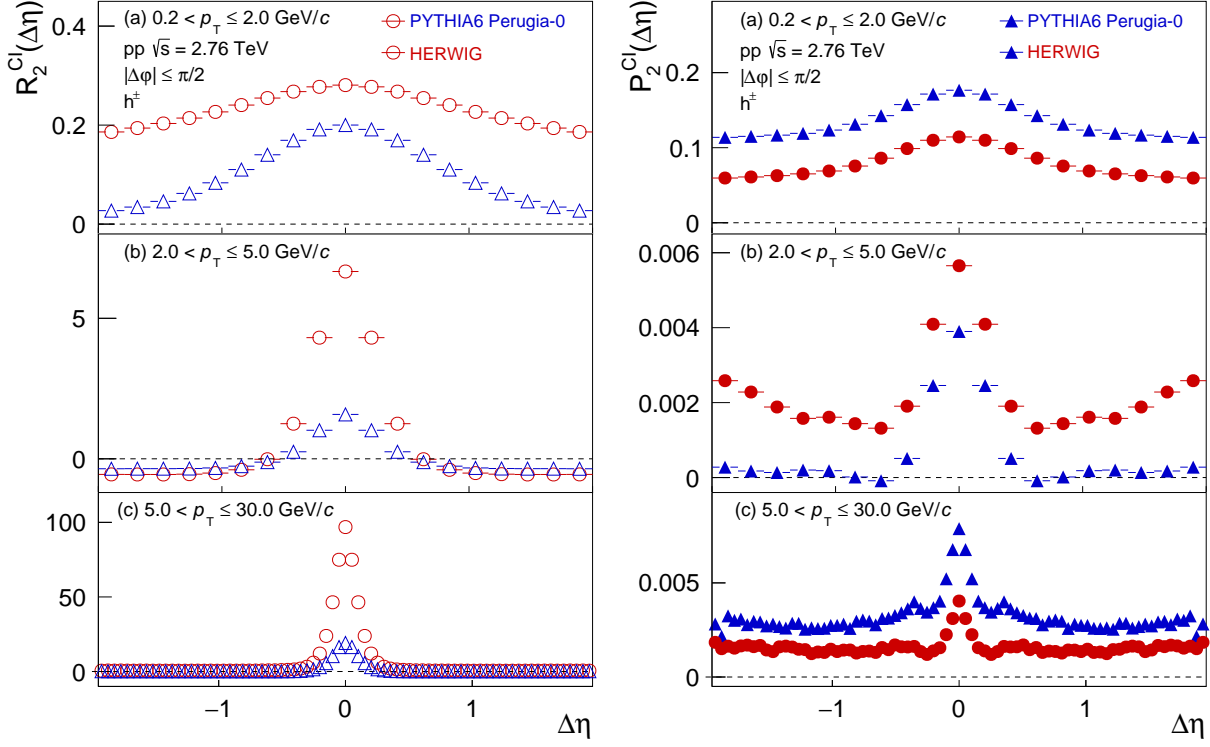


FIG. 5. Projections onto  $\Delta\eta$  of the  $R_2^{\text{CI}}$  (left panel) and  $P_2^{\text{CI}}$  (right panel) correlation functions calculated with PYTHIA (blue) and HERWIG (red) for  $h^\pm$  in pp collisions at  $\sqrt{s} = 2.76$  TeV in selected  $p_T$  ranges. The  $\Delta\eta$  projections are calculated as averages of the two-dimensional correlations in the ranges  $|\Delta\varphi| \leq \pi/2$ .

needed, however, because of the complicated dependence of the correlation strength on the distance to the centroid of the peak. One observes, in particular, that the correlation strength of  $P_2^{\text{CI}}$  exhibits an undershoot, in both  $\Delta\eta$  and  $\Delta\varphi$  projections, in the  $p_T$  range 2.0 - 5.0 GeV/c, and a longer range oscillatory behavior in projections of  $P_2^{\text{CI}}$  along  $\Delta\eta$  in the  $p_T$  range 5.0 - 30.0 GeV/c, as expected from the angular ordering of particle  $p_T$  discussed in sec. II. While difficult to resolve, a hint for the existence of such undershoot feature has already been reported in [28]. The presence of this undershoot stems from the explicit dependence of the correlator on the particles' transverse momentum deviation from the mean, i.e.,  $\Delta p_T \Delta p_T$ . At short angular distance (both longitudinally and azimuthally), jet particles have momenta that tend to exceed the mean  $p_T$  and thus contribute positively, on average, to the correlator. The presence of the undershoot indicates that there is an angular range within which the product  $\Delta p_T \Delta p_T$  is negative on average in PYTHIA events, but shifted in HERWIG events. The shift observed in HERWIG events likely results from larger event-by-event multiplicity fluctuations. At large angular separation, both particles tend to have  $p_T$  below the  $\langle p_T \rangle$  and thus contribute positively to the  $P_2$  correlator. The peak and oscillatory behavior are thus determined by the  $p_T$  and angular ordering of the jet constituents. Given PYTHIA and HERWIG produce particles using a different ordering, they are expected and indeed observed to yield different shapes for the  $P_2$  correlation function. By contrast, the  $R_2$  correlation function receives positive definite contributions from all particle pairs of a jet and is thus not sensitive to the ordering of the particles of the pair but only the overall width of the jet. Measurements of  $R_2$  and  $P_2$  correlation functions in p-Pb and Pb-Pb collisions shall thus provide better discriminants of the parton splitting and hadronization mechanisms at play in jet fragmentation as well as in the generation of the underlying event.

The  $R_2^{\text{CI}}$  and  $P_2^{\text{CI}}$  correlations also exhibit stark differences on the away-side, i.e., at  $\Delta\varphi \sim \pi$ . Inspection of the away-side of the  $R_2$  (Fig. 3) and  $P_2$  correlation functions (Fig. 4), and their  $\Delta\varphi$  projections (Fig. 6)



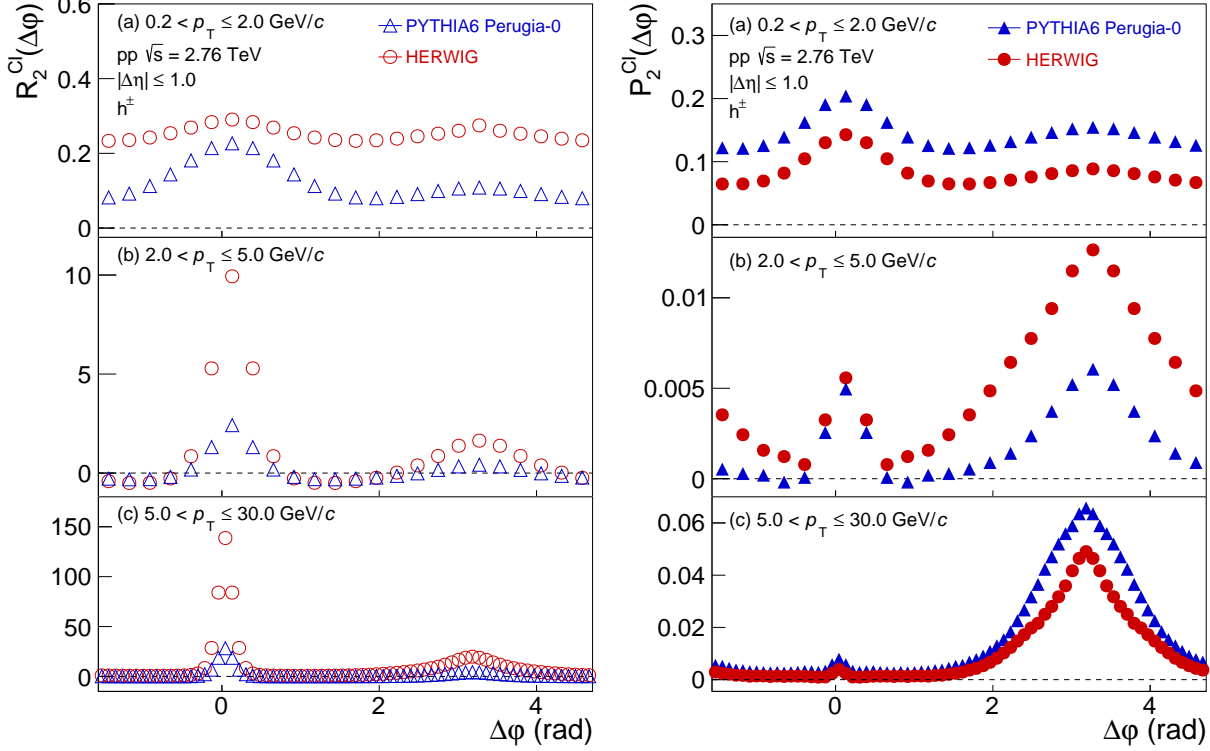


FIG. 6. Projections onto  $\Delta\varphi$  of  $R_2^{CI}$  (left panel) and  $P_2^{CI}$  (right panel) correlation functions calculated with PYTHIA (blue) and HERWIG (red) for  $h^\pm$  in pp collisions at  $\sqrt{s} = 2.76$  TeV in selected  $p_T$  ranges. The  $\Delta\varphi$  projections are calculated as averages of the two-dimensional correlations in the ranges  $|\Delta\eta| \leq 1.0$ .

reveal the two correlators yield a rather different response to the away-side jet. Indeed, the away-side jet yields a relatively modest ridge-like structure at  $\Delta\varphi \sim \pi$  in  $R_2$  correlation functions but produces a very large amplitude away-side in  $P_2$ . One also finds that PYTHIA and HERWIG produce away-side ridges with different shapes and strengths as well as quantitatively different  $p_T$  dependence. Comparative measurements of the  $R_2$  and  $P_2$  correlators in different particle momentum ranges in pp collisions should thus provide additional insight and constraints on the hadronization mechanisms implemented in these models.

## 2. Charge Dependent Correlations

We next shift our attention to the CD correlation functions presented in Figs. 7 and 9.

These were obtained by subtraction of the LS correlations from the US correlations according to Eq. (9). As such, they emphasize the role of charge conservation in particle production. Correlation functions  $R_2$  (and similarly charge balance functions) indeed provide signatures of the charged particle pair production and transport in pp and A–A collisions. For instance, at momenta in excess of 2.0 GeV/c, as shown in Fig. 7 (b,c), one observes the correlator  $R_2$  features an isolated peak centered at  $(\Delta\eta, \Delta\varphi) = (0, 0)$  resulting from the fact that correlated charged particle production occurs almost exclusively within the confines of a single jet.

The width of the peak decreases monotonically with increasing particle momentum owing to the Schwinger mechanism and angular ordering discussed in sec. II. At lower momenta, however, correlated charged pair production may occur over a wider range of angles, even back-to-back, as illustrated by the very sharp and narrow away-side ridge predicted by HERWIG in the range  $0.2 \leq p_T \leq 2.0$  GeV/c.

PYTHIA6 Perugia-0, pp  $\sqrt{s} = 2.76$  TeV

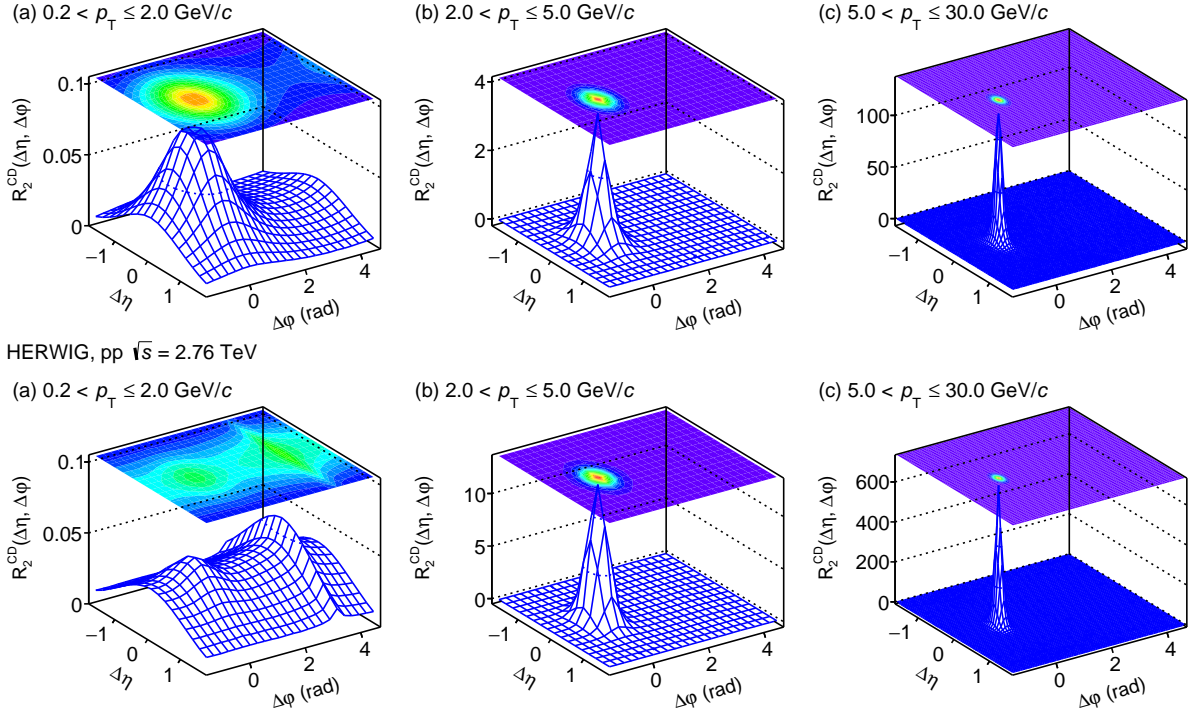


FIG. 7. Correlation functions  $R_2^{\text{CD}}$  of charged hadrons, in selected  $p_T$  ranges, obtained with PYTHIA (top panel) and HERWIG (bottom panel) in pp collisions at  $\sqrt{s} = 2.76$  TeV.

HERWIG, pp  $\sqrt{s} = 2.76$  TeV  
 $0.2 < p_T \leq 2.0$  GeV/c,  $N_{\text{total}} > 50$

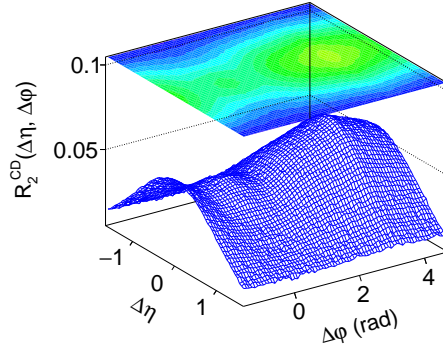


FIG. 8. Correlation function  $R_2^{\text{CD}}$  obtained with HERWIG for charged hadrons in pp collisions at  $\sqrt{s} = 2.76$  TeV with a minimum multiplicity cut,  $N_{\text{total}} > 50$ .

The  $R_2^{\text{CD}}$  correlation functions obtained with PYTHIA (top panels) and HERWIG (bottom panels) for particles in the range  $0.2 \leq p_T \leq 2.0$  GeV/c indeed feature a more complicated shape involving both a near-side peak and an away-side structure. In this case, one notes that PYTHIA and HERWIG produce very different predictions, owing most likely to their different implementation of the underlying event. Additionally note, as exemplified in Fig. 7, that the shape and strength of  $R_2^{\text{CD}}$  exhibit a strong depen-

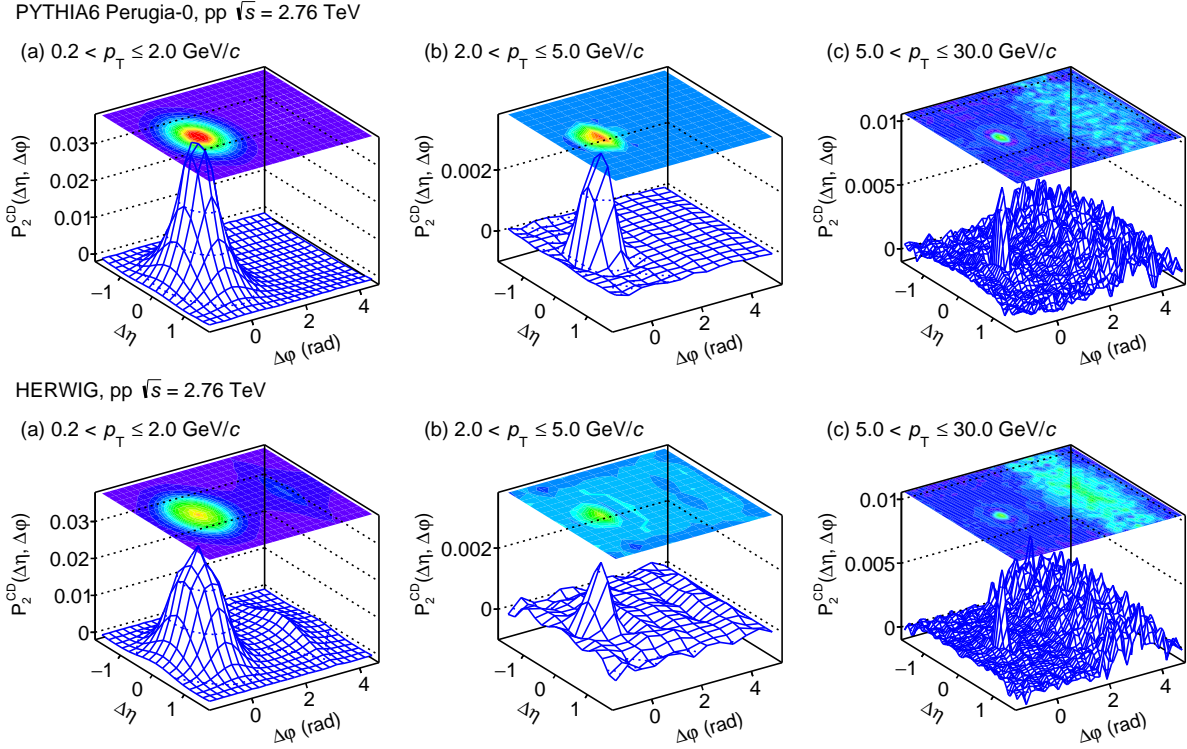


FIG. 9. Correlation functions  $P_2^{\text{CD}}$  of charged hadrons, in selected  $p_T$  ranges, obtained with PYTHIA (top panel) and HERWIG (bottom panel) in pp collisions at  $\sqrt{s} = 2.76$  TeV.

dence on the produced hadron multiplicity. Measurements of  $R_2^{\text{CD}}$  in pp collisions for various momentum and produced particle multiplicity ranges shall then provide very useful constraints in the tuning of these models.

The PYTHIA and HERWIG predictions for  $P_2^{\text{CD}}$  correlation functions, shown in Fig. 9, indicate this correlator is also of interest to probe the internal structure of jets and the charge production ordering. With PYTHIA, the near-side peak of the  $P_2^{\text{CD}}$  correlation functions is significantly narrower than its  $R_2^{\text{CD}}$  counterpart in the lowest  $p_T$  range considered, but somewhat wider at higher  $p_T$ . By contrast, HERWIG's predictions of  $P_2^{\text{CD}}$  features a somewhat narrower near-side peak in all three momentum ranges. One also notes that the near-side predicted by PYTHIA and HERWIG have different shapes, widths, and a somewhat complicated dependence on the  $p_T$  of the particles. One finds additionally that the away-side of  $P_2^{\text{CD}}$  correlation functions feature a large amplitude for high- $p_T$  particles. This is in stark contrast to the  $R_2^{\text{CD}}$  correlation functions that feature an almost flat away-side yield. Such a small away-side yield is expected in  $R_2^{\text{CD}}$  owing to the fact that particle production above  $p_T \geq 2$  GeV/c is dominated by jet fragmentation. Given charge is conserved locally in the jet fragmentation process, one can expect, on general grounds, that charge correlations between jets, if any, are driven primarily by the charge of the parton that initiate the jets. Quark jets may be charge correlated but jets initiated by gluons should not be, at least to first order. Measurements of the  $P_2^{\text{CD}}$  away-side strength thus provide an additional tool to probe the nature of the jets measured in pp and A–A collisions. Indeed, back-to-back gluon jets should yield no contributions to the away-side of  $P_2^{\text{CD}}$  correlation functions but quark-quark jet pairs should have a finite CD correlation. The measured away-side yield of  $P_2^{\text{CD}}$  correlation functions may thus provide a new tool to determine the origin and nature of jets measured in elementary collisions.

We note that the  $R_2^{\text{CD}}$  correlator computed with HERWIG in the range  $0.2 < p_T \leq 2.0$  GeV/c, shown in Fig. 7, features a narrow elongated structure at  $\Delta\phi = \pi$ . This structure likely corresponds to underlying

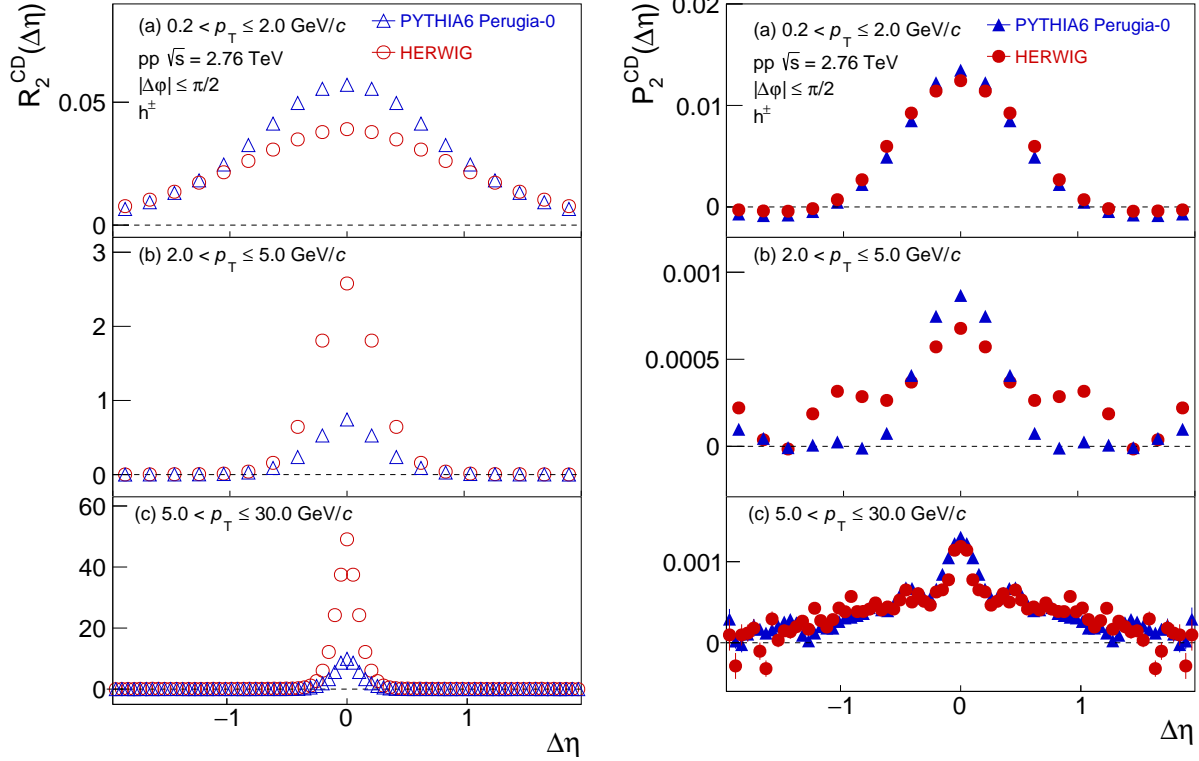


FIG. 10. Projections onto  $\Delta\eta$  of  $R_2^{\text{CD}}$  (left column) and  $P_2^{\text{CD}}$  (right column) correlation functions of charged hadrons calculated in selected  $p_T$  ranges with PYTHIA (blue) and HERWIG (red) in pp collisions at  $\sqrt{s} = 2.76$  TeV. The projections are calculated as averages of the two-dimensional correlations in the range  $|\Delta\varphi| \leq \pi/2$ .

event particle pairs emitted back-to-back in the laboratory frame and are likely produced in excess given such a structure is not observed in data reported by the ALICE collaboration [28]. We find, however, that contributions of such pairs to the correlator are suppressed in HERWIG events featuring a total particle multiplicity  $N_{\text{total}} > 50$  in the fiducial acceptance, as shown in Fig. 8. An experimental investigation of  $R_2^{\text{CD}}$  and  $P_2^{\text{CD}}$  correlation functions as a function of pp collision multiplicity is thus of obvious interest to elucidate the role and interplay of underlying events and multi-jet production in these collisions.

### B. Transverse momentum dependence of the width of the CI and CD near-side peaks

We study the  $p_T$  evolution of the RMS widths of the near-side peaks of the  $R_2$  and  $P_2$  correlation functions obtained with PYTHIA and HERWIG. The  $\Delta\eta$  and  $\Delta\varphi$  RMS widths are calculated according to

$$\sigma_{\Delta\eta} = \left( \frac{\sum_{i,j} [O(\Delta\eta_i, \Delta\varphi_j) - O_{\text{offset}}] \Delta\eta_i^2}{\sum_{i,j} O(\Delta\eta_i, \Delta\varphi_j)} \right)^{1/2}, \quad (11)$$

$$\sigma_{\Delta\varphi} = \left( \frac{\sum_{i,j} [O(\Delta\eta_i, \Delta\varphi_j) - O_{\text{offset}}] \Delta\varphi_i^2}{\sum_{i,j} O(\Delta\eta_i, \Delta\varphi_j)} \right)^{1/2}, \quad (12)$$

where  $O(\Delta\eta_i, \Delta\varphi_j)$  represent the strength of the correlation functions in bins  $\Delta\eta_i$  and  $\Delta\varphi_j$  and the sums on  $\Delta\eta_i$  covers the  $|\Delta\eta| \leq 1.0$  acceptance of the simulation, whereas the sums on  $\Delta\varphi_i$  are limited to exclude the away-side ridge. Offsets are used to suppress negative correlation values and eliminate trivial

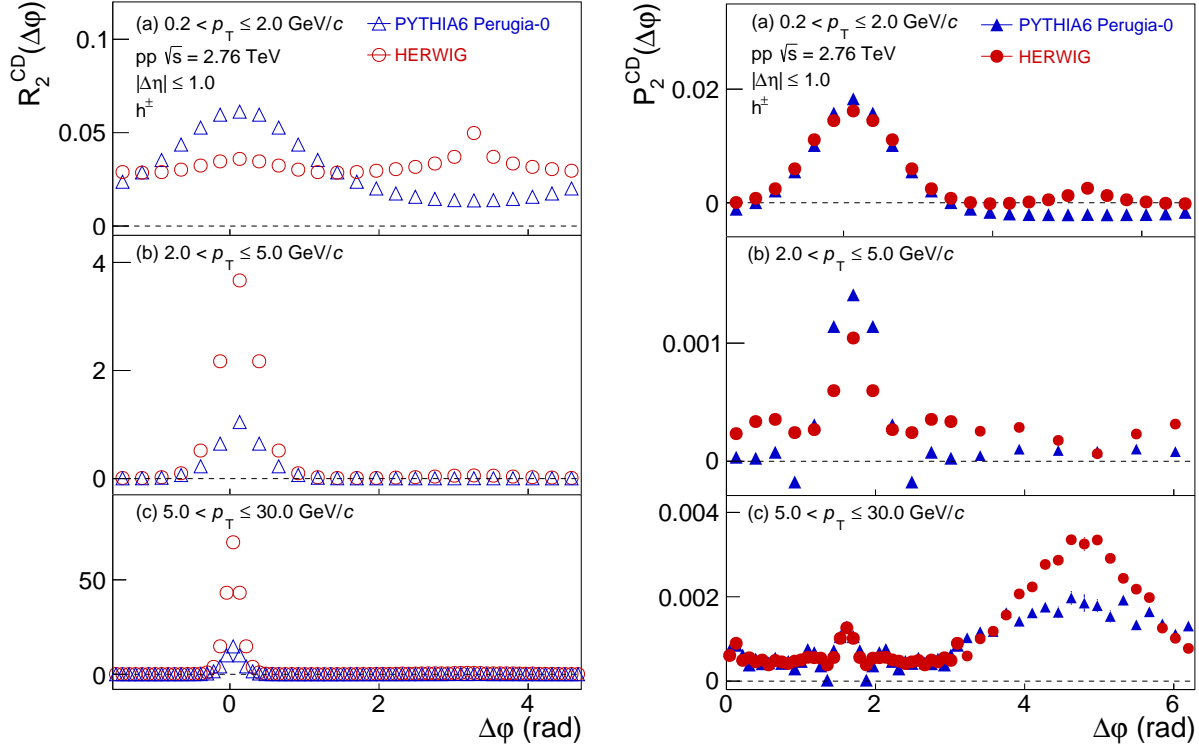


FIG. 11. Projections onto  $\Delta\varphi$  of  $R_2^{\text{CD}}$  (left column) and  $P_2^{\text{CD}}$  (right column) correlation functions of charged hadrons calculated in selected  $p_T$  ranges with PYTHIA (blue) and HERWIG (red) in pp collisions at  $\sqrt{s} = 2.76$  TeV. The  $\Delta\varphi$  projections are calculated as averages of the two-dimensional correlations in the range  $|\Delta\eta| \leq 1.0$ .

width values determined by the breadth of the acceptance. They are obtained by taking the average of three bins at the edge of the acceptance, i.e., at  $|\Delta\eta| = 2.0$  for  $\Delta\eta$  projections, and at the minimum of the correlations, near  $\Delta\varphi = -\pi/2$ , for  $\Delta\varphi$  projections. The three-bin average technique is also used for calculating offsets whenever undershoots are present in  $P_2$  correlators.

Figures 12 and 13 present plots of the evolution of the  $\Delta\eta$  and  $\Delta\varphi$  widths of the near-side peak of CI and CD correlators as a function of  $p_T$ . Overall, one finds the widths decrease with rising  $p_T$ . However, widths obtained with PYTHIA exhibit a smooth and monotonic behavior with increasing particle  $p_T$  whereas widths obtained from HERWIG exhibit a more complicated  $p_T$  dependence. This study reveals an interesting case where the  $P_2$  width is broader than that of  $R_2$  in some  $p_T$  ranges, in stark contrast with the results reported in [28].

In order to further understand the structures observed in  $R_2$  and  $P_2$  correlation functions presented in Fig. 3 - 9, we study, in Figs. 14 and 15, the evolution of the near-side peak of the correlators as a function of the total particle multiplicity  $N_{\text{total}}$ . We find that the longitudinal and azimuthal widths,  $\sigma_{\Delta\eta}$  and  $\sigma_{\Delta\varphi}$ , of the  $R_2^{\text{CI}}$ ,  $R_2^{\text{CD}}$ , and  $P_2^{\text{CD}}$  correlators are slowly varying functions of  $N_{\text{total}}$ , with largest dependence observed for the width  $\sigma_{\Delta\varphi}$  predicted by HERWIG for particles in the range  $0.2 < p_T \leq 2.0$  GeV/c. The widths of the  $P_2^{\text{CI}}$  correlator, on the other hand, exhibit a more complicated dependence on  $N_{\text{total}}$ . One observes, indeed, that the widths extracted both from PYTHIA and HERWIG exhibit a discontinuity near or above  $N_{\text{total}} = 30$ , thereby signaling a drastic change in the shape of these correlation functions between low and high multiplicity events. The shape dependence on  $N_{\text{total}}$  is illustrated in Fig. 16. Events of low multiplicity feature  $P_2^{\text{CI}}$  correlator with a clear undershoot structure, yielding narrow widths in both the longitudinal and azimuthal directions. As argued above, the undershoot structure is associated with the production of pairs featuring  $\Delta p_T \Delta p_T < 0$  but multiplicity fluctuations shift the correlator, globally, to positive values. The number of such pair combinations is manifestly reduced, however, for

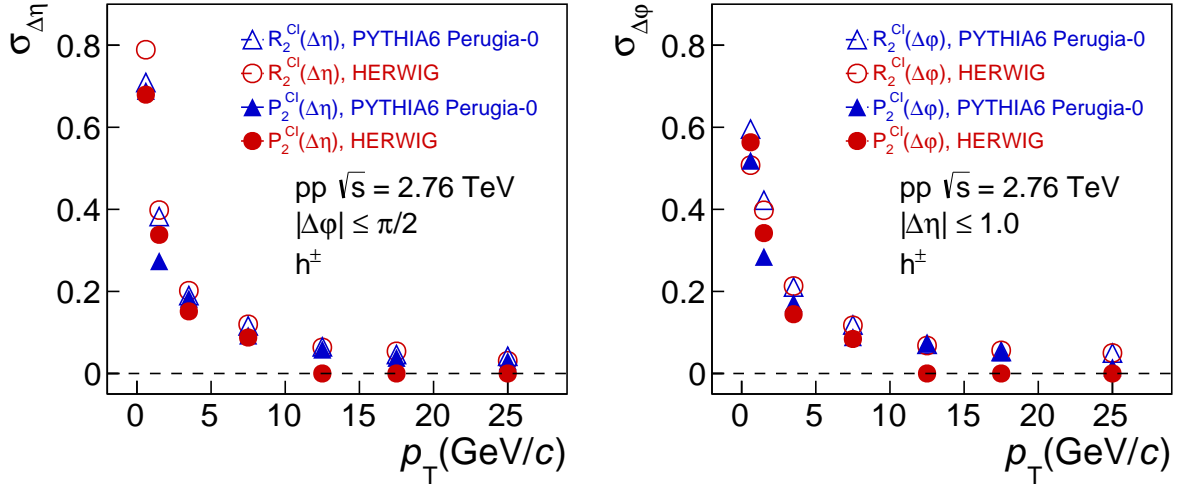


FIG. 12. Width of the near-side peak of CI correlation functions along  $\Delta\eta$  (left panel), in the range  $|\Delta\phi| \leq \pi/2$ , and along  $\Delta\phi$  (right panel), in the range  $|\Delta\eta| \leq 1.0$ , as function of the momentum of the particles.

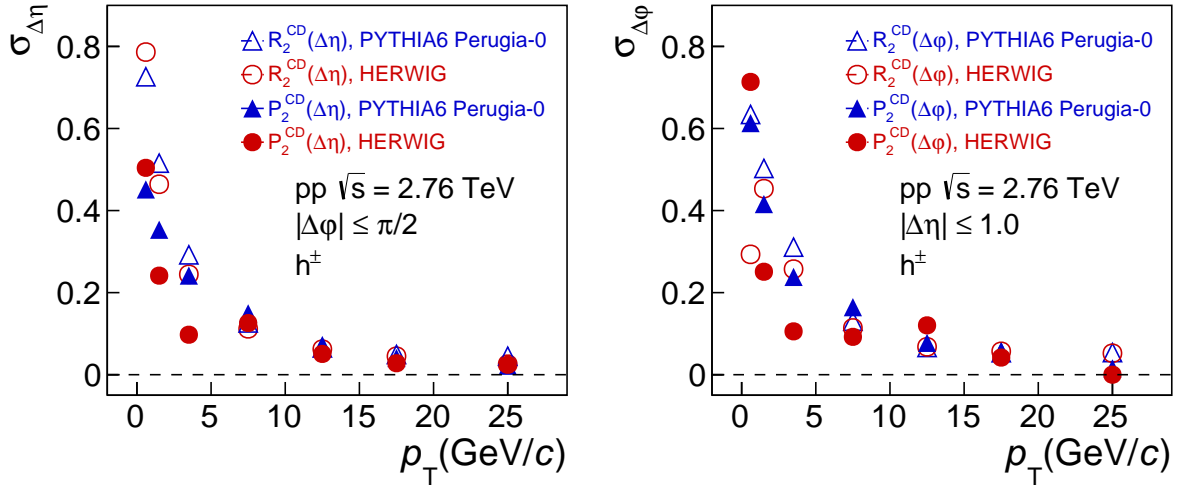


FIG. 13. Width of the near-side peak of CD correlation functions along  $\Delta\eta$  (left panel), in the range  $|\Delta\phi| \leq \pi/2$ , and along  $\Delta\phi$  (right panel), in the range  $|\Delta\eta| \leq 1.0$ , as function of the momentum of the particles.

collisions with large  $N_{\text{total}}$ . These consequently do not feature an undershoot behavior and thus produce a broad near-side peak. This behavior likely stems from the fact that high-multiplicity events favor gluon jets. These are less collimated than quark jets and feature softer particles on average [52]. Evidently, such variations are not possible with the  $R_2^{\text{CI}}$  correlators. We thus conclude that the  $P_2^{\text{CI}}$  correlator constitutes a more discriminating probe of the correlation structure of jets and their underlying events than the  $R_2^{\text{CI}}$  correlator.

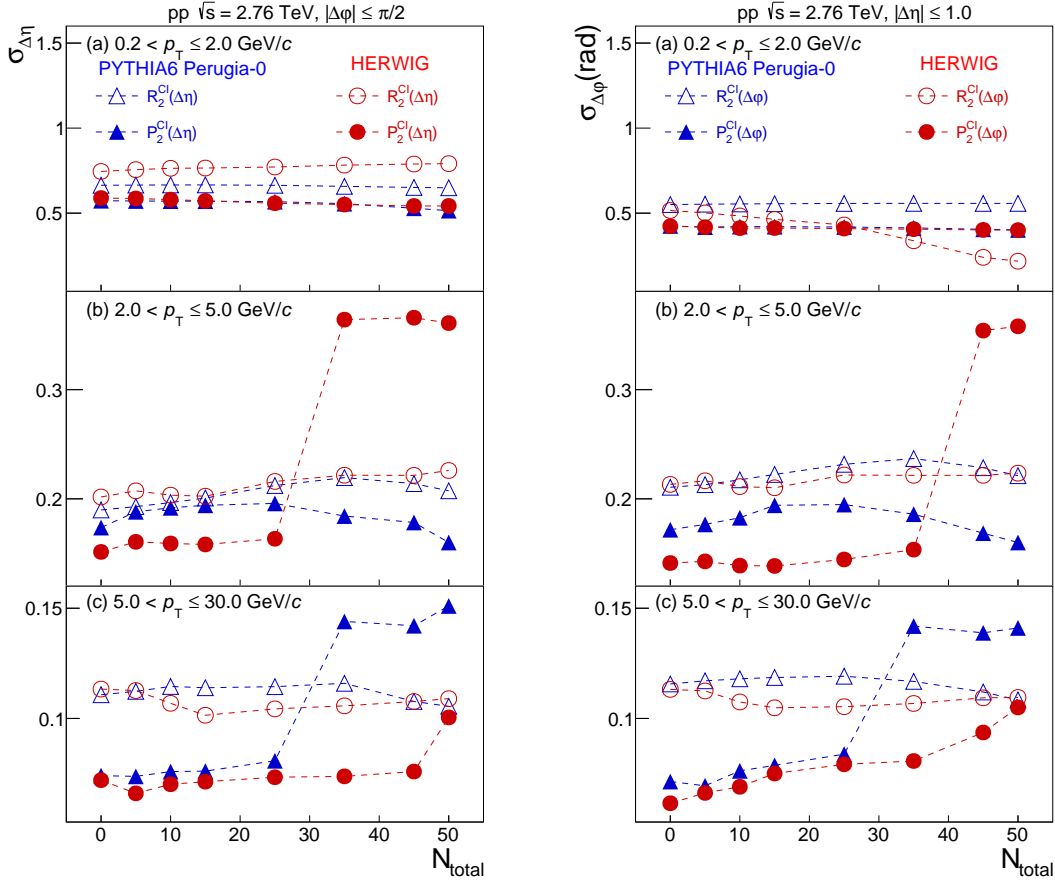


FIG. 14. Width of the near-side peak of CI correlation functions along  $\Delta\eta$  (left panel), in the range  $|\Delta\phi| \leq \pi/2$ , and along  $\Delta\phi$  (right panel), in the range  $|\Delta\eta| \leq 1.0$ . Dotted lines are drawn to guide the eye.

### C. Identified charged hadron correlations

Experimental studies at the ISR, FNAL, and the LHC have shown that jet fragmentation functions of identified species vary appreciably between mesons and baryons as well as with their quark content ([53] and references therein). Unfortunately, measuring the fragmentation functions of identified hadron species within jets is a statistically onerous and difficult task, specially for high- $z$  particles in high-energy jets. Measuring the strength and shape of  $R_2^{CI}$ ,  $P_2^{CI}$ ,  $R_2^{CD}$ , and  $P_2^{CD}$  correlation functions of identified high- $p_T$  hadrons, however, may provide an invaluable proxy to such studies. We proceed to substantiate this hypothesis by studying the shape and strength of identified hadron correlation functions based on predictions by the PYTHIA and HERWIG models. Figures 17 and 18 respectively display  $R_2^{CI}$  and  $P_2^{CI}$  correlation functions calculated with PYTHIA for  $\pi^\pm$ ,  $K^\pm$  and  $p\bar{p}$ , in the range  $0.2 < p_T \leq 2.0$  GeV/ $c$ .

Again in the case of identified particles, one observes that the width of the near-side peak of the  $P_2^{CI}$  correlator is significantly narrower than its  $R_2^{CI}$  counterpart. However, the shape and width of these two correlators do not exhibit a monotonic dependence on the mass of the particles. For kaons, in particular, both  $R_2^{CI}$  and  $P_2^{CI}$  feature a near-side peak that might be perhaps best described by a superposition of a wide and a narrow Gaussian peak, which arises, in part, from a strong admixture of  $\phi$ -meson decays. A similar situation arises for  $R_2^{CD}$  and  $P_2^{CD}$  shown in Figs. 19 and 20, respectively. One finds, for all three particle species, that the near-side peak of the  $P_2^{CD}$  correlators are markedly narrower than their  $R_2^{CD}$  counterparts. One also observes that the kaon near-side peaks are much narrower than those of pions and protons. It is also worth noticing that the pion  $R_2^{CD}$  correlator shows a rather large away-

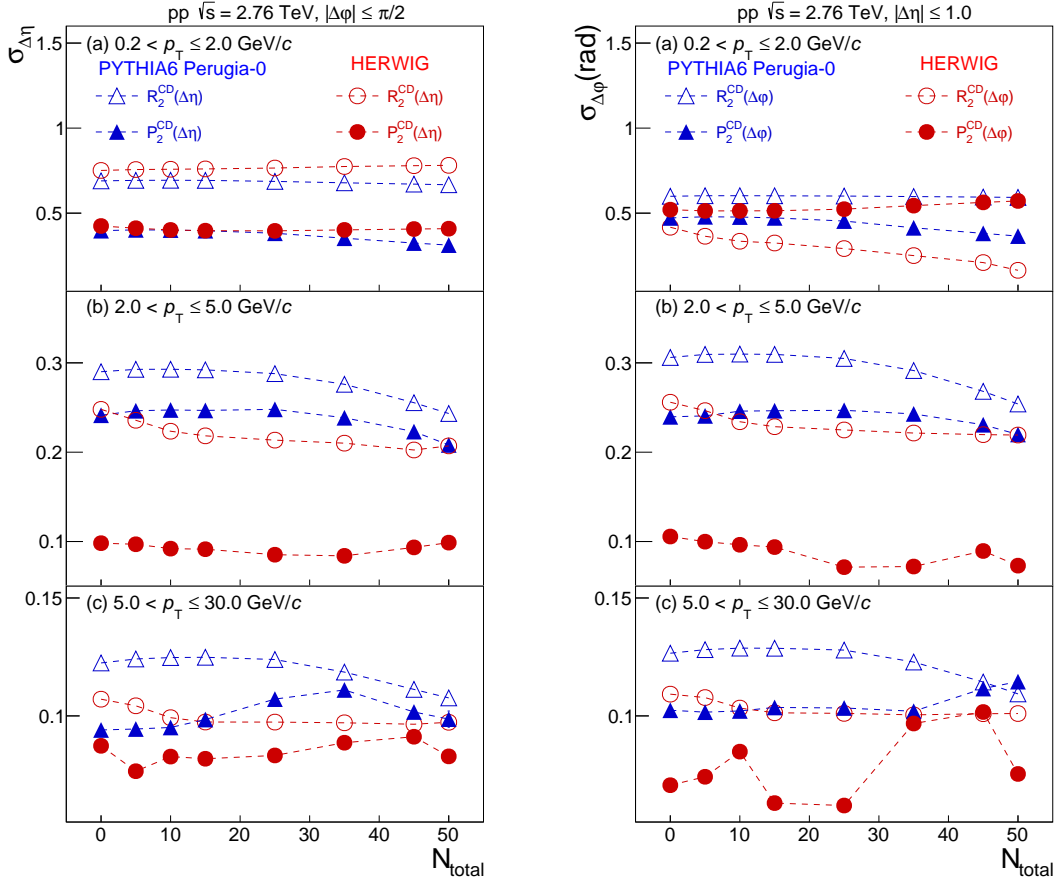


FIG. 15. Width of the near-side peak of CD correlation functions along  $\Delta\eta$  (left panel), in the range  $|\Delta\varphi| \leq \pi/2$ , and along  $\Delta\varphi$  (right panel), in the range  $|\Delta\eta| \leq 1.0$ . Dotted lines are drawn to guide the eye.

side amplitude (relative to its near-side peak amplitude) while kaons and protons feature much smaller relative away-side amplitudes for this correlator. By contrast, all three species have a flat and nearly vanishing away-side amplitude in  $P_2^{\text{CD}}$  within PYTHIA simulations (Fig. 20) for particles within  $0.2 < p_T \leq 2.0$  GeV/c. Qualitatively similar conclusions are obtained from calculations of the  $R_2$  and  $P_2$  correlators with HERWIG in this momentum range (2D plots not shown). Indeed, projections of the  $R_2$  and  $P_2$  correlation functions obtained with PYTHIA and HERWIG, shown in Figs. 21-24, illustrate that while the predictions of the two models are qualitatively similar, they differ quantitatively for the three particle species considered. It is very difficult to study this in other  $p_T$  regions for RMS width calculation because of large oscillating behavior in  $P_2^{\text{CD}}$   $p\bar{p}$  in the  $p_T$  range 2.0 - 5.0 GeV/c. An actual measurement of such correlation functions (possible at the LHC with the ALICE detector) shall thus provide significant constraints to tune these models and achieve a better understanding of particle production processes in elementary particle collisions.

## V. SUMMARY

We presented a study of charge-independent and charge-dependent two-particle differential- number correlation functions  $R_2$  and transverse momentum correlation functions  $P_2$  in pp collisions at  $\sqrt{s} = 2.76$  TeV with the PYTHIA and HERWIG Monte Carlo models. Calculations were presented for unidentified hadrons as well as for  $\pi^\pm$ ,  $K^\pm$  and  $p\bar{p}$  individual species in selected ranges of transverse momentum.



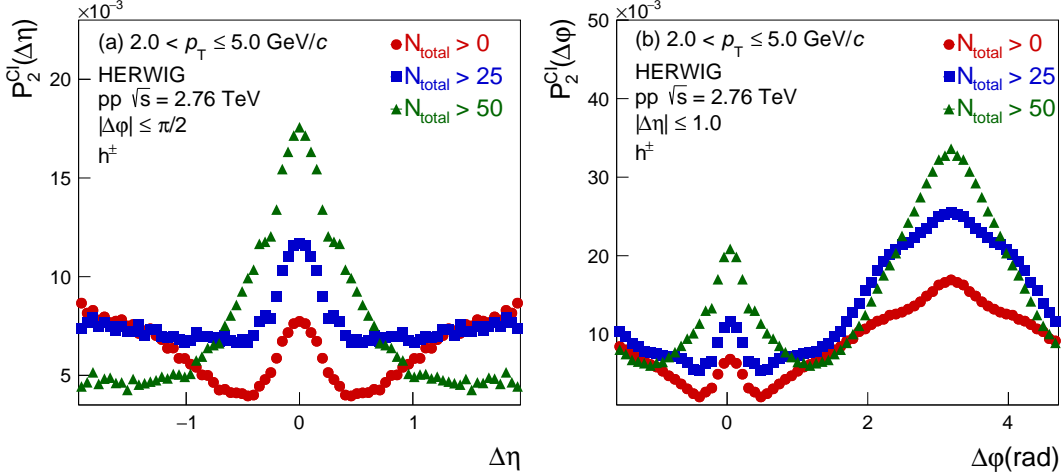


FIG. 16. Projections onto  $\Delta\eta$  (left panel) and  $\Delta\varphi$  (right panel) of the  $P_2^{\text{CI}}$  correlation functions calculated with HERWIG for  $h^\pm$  in the  $p_T$  range 2.0 - 5.0 GeV/c in pp collisions at  $\sqrt{s} = 2.76$  TeV for 3 different  $N_{\text{total}}$  cuts. The  $\Delta\eta$  and  $\Delta\varphi$  projections are calculated as averages of the two-dimensional correlations in the ranges  $|\Delta\varphi| \leq \pi/2$  and  $|\Delta\eta| \leq 1.0$ , respectively.

PYTHIA6 Perugia-0, pp  $\sqrt{s} = 2.76$  TeV  
 $0.2 < p_T \leq 2.0$  GeV/c

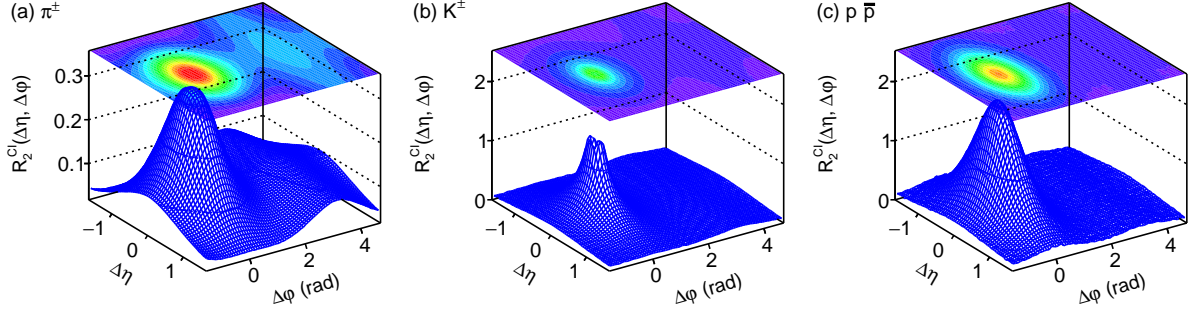


FIG. 17. Correlation functions  $R_2^{\text{CI}}$  of  $\pi^\pm$ ,  $K^\pm$  and  $p\bar{p}$ , within  $|\eta| < 1.0$  and  $0.2 < p_T \leq 2.0$  GeV/c, obtained with PYTHIA in pp collisions at  $\sqrt{s} = 2.76$  TeV.

PYTHIA and HERWIG both qualitatively reproduce the near-side peak and away-side ridge correlation features reported by experiments. At low  $p_T$ , both models produce narrower near-side peaks in  $P_2$  correlations than in  $R_2$  as reported by the ALICE collaboration in p-Pb and Pb-Pb collisions [28]. This suggests that the narrower shape of the  $P_2$  near-side peak is largely determined by the  $p_T$  dependent angular ordering of hadrons produced in jets, as discussed in sec. II. We have provided detailed calculations of the longitudinal and azimuthal widths of the near-side peak as a reference to prospective experimental studies of these correlation functions. Both PYTHIA and HERWIG predict widths that decrease with increasing  $p_T$ . Widths extracted for  $P_2$  correlators are typically significantly narrower than those of the  $R_2$  counterparts. We also showed that the models predict non-trivial dependence on the mass of identified particles arising in part from resonance decays.

We additionally find that the models produce large amplitude ridge structures at  $\Delta\varphi = \pi$  in  $P_2$  correlation functions while yielding relatively modest ridges in  $R_2$ . The amplitude of the ridge structure in  $P_2^{\text{CI}}$  is found to increase with the particle  $p_T$  range considered reaching rather large amplitude for particles in the  $5.0 < p_T \leq 30.0$  GeV/c range. An away-side ridge is also observed in  $P_2^{\text{CD}}$  correlation

PYTHIA6 Perugia-0, pp  $\sqrt{s} = 2.76$  TeV

$0.2 < p_T \leq 2.0$  GeV/c

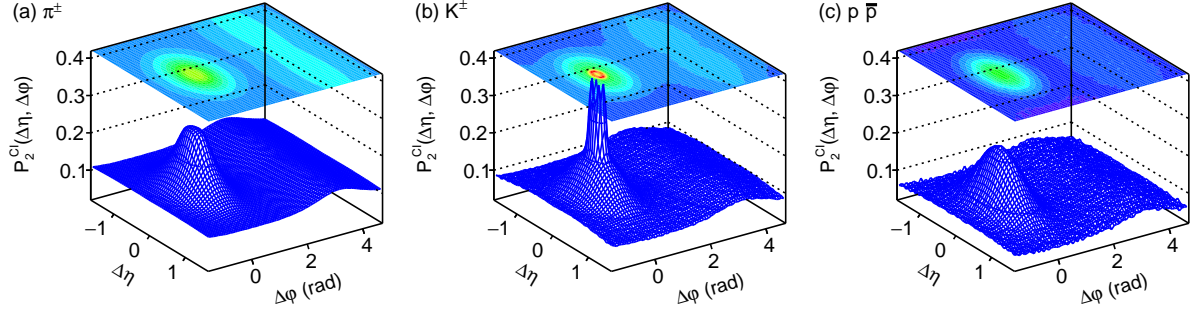


FIG. 18. Correlation functions  $P_2^{CI}$  of  $\pi^\pm$ ,  $K^\pm$  and  $p\bar{p}$ , within  $|\eta| < 1.0$  and  $0.2 < p_T \leq 2.0$  GeV/c, obtained with PYTHIA in pp collisions at  $\sqrt{s} = 2.76$  TeV.

PYTHIA6 Perugia-0, pp  $\sqrt{s} = 2.76$  TeV

$0.2 < p_T \leq 2.0$  GeV/c

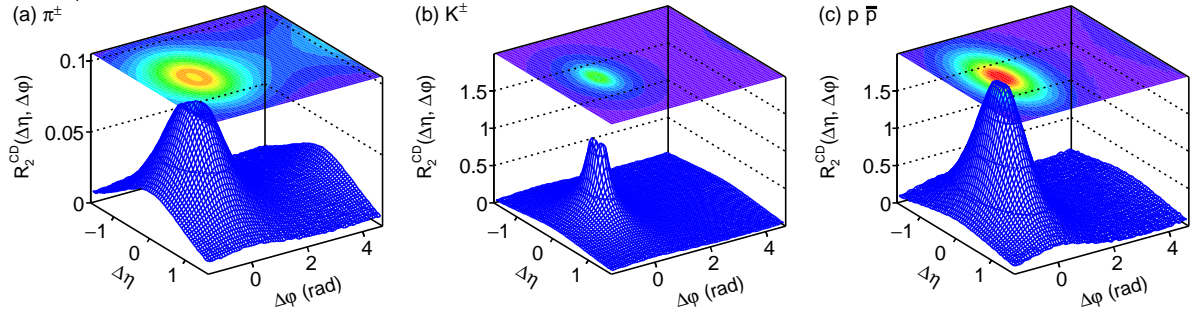


FIG. 19. Correlation functions  $R_2^{CD}$  of  $\pi^\pm$ ,  $K^\pm$  and  $p\bar{p}$ , within  $|\eta| < 1.0$  and  $0.2 < p_T \leq 2.0$  GeV/c, obtained with PYTHIA in pp collisions at  $\sqrt{s} = 2.76$  TeV.

PYTHIA6 Perugia-0, pp  $\sqrt{s} = 2.76$  TeV

$0.2 < p_T \leq 2.0$  GeV/c

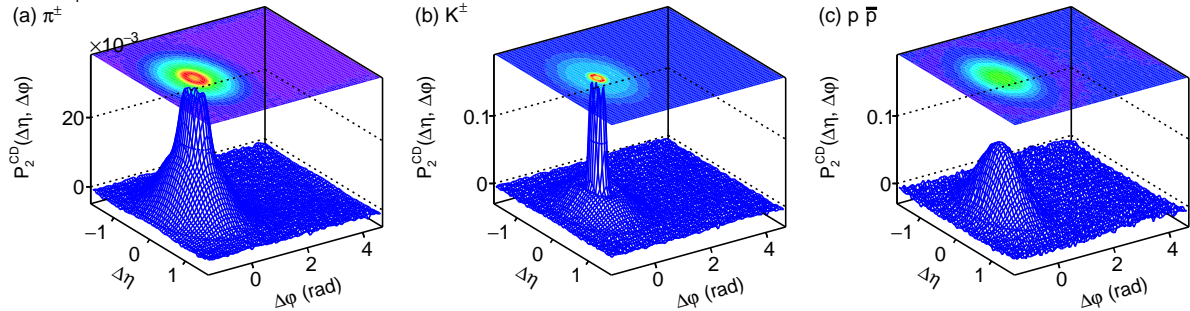


FIG. 20. Correlation functions  $P_2^{CD}$  of  $\pi^\pm$ ,  $K^\pm$  and  $p\bar{p}$ , within  $|\eta| < 1.0$  and  $0.2 < p_T \leq 2.0$  GeV/c, obtained with PYTHIA in pp collisions at  $\sqrt{s} = 2.76$  TeV.

functions. The magnitude of this ridge shall depend on jet-to-jet charge correlations. Measurements of  $P_2^{CD}$  correlation functions of high- $p_T$  particles in pp collisions might then be sensitive to the charge of the partons initiating the observed jets. Elucidation of this conjecture, however, requires further studies, with both PYTHIA and HERWIG, of the correlation functions obtained when jet production is restricted

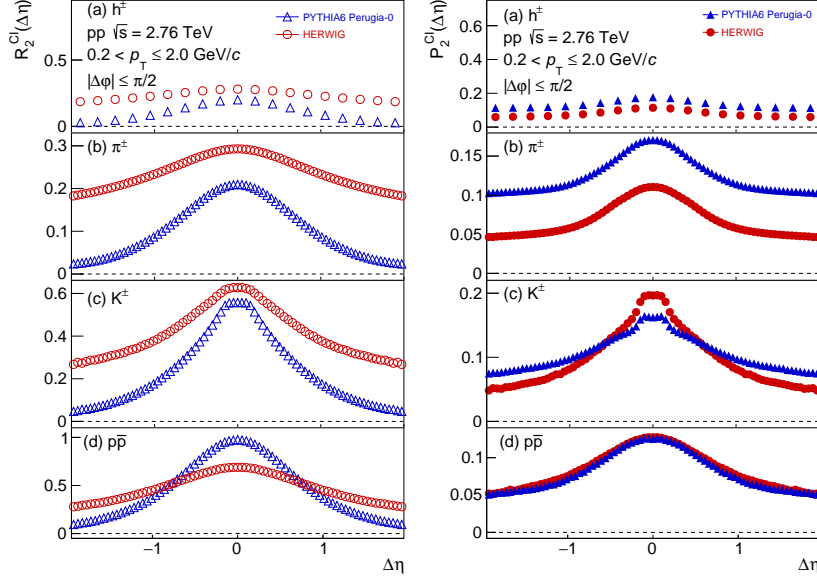


FIG. 21. Projections onto  $\Delta\eta$  of  $R_2^{\text{CI}}$  (left column) and  $P_2^{\text{CI}}$  (right column) correlation functions of  $h^\pm$ ,  $\pi^\pm$ ,  $K^\pm$  and  $p\bar{p}$  calculated with PYTHIA (blue) and HERWIG (red) in pp collisions at  $\sqrt{s} = 2.76$  TeV. The projections are calculated as averages of the two-dimensional correlations in the range  $|\Delta\varphi| \leq \pi/2$ .

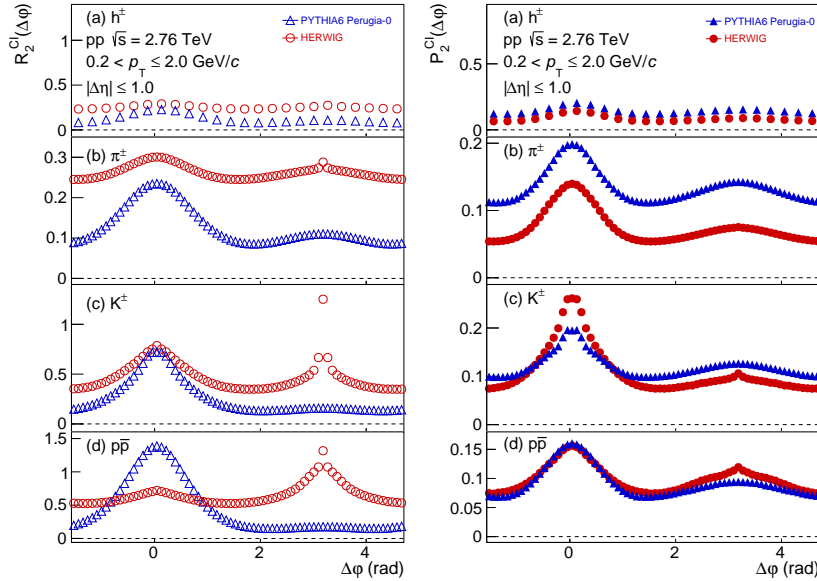


FIG. 22. Projections onto  $\Delta\varphi$  of  $R_2^{\text{CI}}$  (left column) and  $P_2^{\text{CI}}$  (right column) correlation functions of  $h^\pm$ ,  $\pi^\pm$ ,  $K^\pm$  and  $p\bar{p}$  calculated with PYTHIA (blue) and HERWIG (red) in pp collisions at  $\sqrt{s} = 2.76$  TeV.

to gluon-gluon or quark-quark processes.

#### ACKNOWLEDGEMENTS

The authors thank Drs. Joern Putschke and Sidharth Prasad for fruitful discussions and their inval-

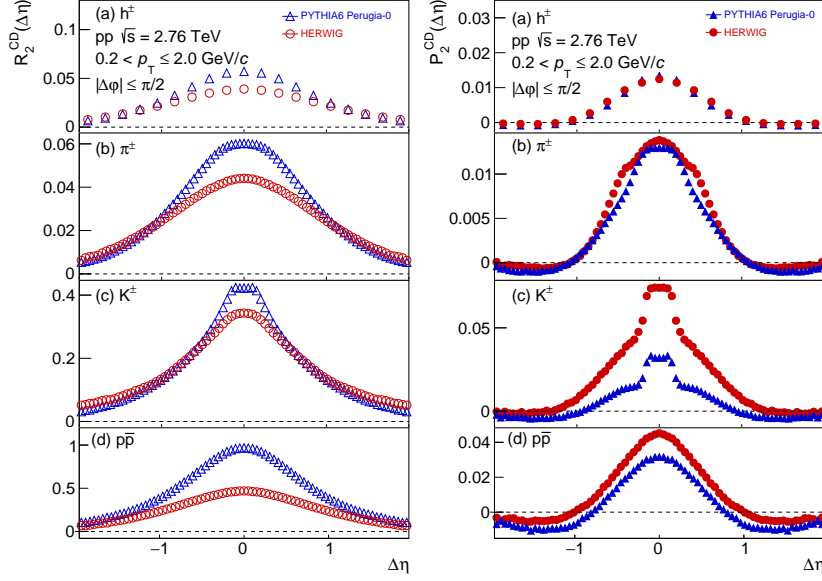


FIG. 23. Projections onto  $\Delta\eta$  of  $R_2^{\text{CD}}$  (left column) and  $P_2^{\text{CD}}$  (right column) correlation functions of  $h^\pm$ ,  $\pi^\pm$ ,  $K^\pm$  and  $p\bar{p}$  calculated with PYTHIA (blue) and HERWIG (red) in pp collisions at  $\sqrt{s} = 2.76$  TeV. The projections are calculated as averages of the two-dimensional correlations in the range  $|\Delta\varphi| \leq \pi/2$ .

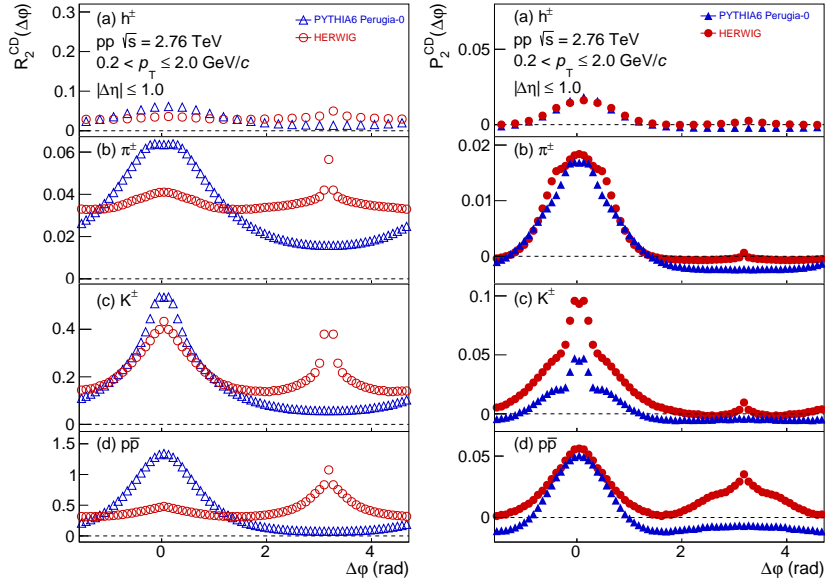


FIG. 24. Projections onto  $\Delta\varphi$  of  $R_2^{\text{CD}}$  (left column) and  $P_2^{\text{CD}}$  (right column) correlation functions of  $h^\pm$ ,  $\pi^\pm$ ,  $K^\pm$  and  $p\bar{p}$  calculated with PYTHIA (blue) and HERWIG (red) in pp collisions at  $\sqrt{s} = 2.76$  TeV.

able review of the manuscript. This work was supported in part by the United States Department of Energy, Office of Nuclear Physics (DOE NP), United States of America, under grant No. DE-FOA-0001664, and the Department of Science and Technology(DST), Government of India, under grants No. SR/MF/PS-01/2014-IITB and SR/MF/PS-02/2014-IITM, as well as the University Grants Commis-

sion(UGC), Government of India, under the Code No. BININ00401340.

- 
- [1] J. Adams *et al.* (STAR Collaboration), Nucl. Phys. **A757**, 102 (2005), arXiv:nucl-ex/0501009 [nucl-ex].
- [2] K. Adcox *et al.* (PHENIX Collaboration), Nucl. Phys. **A757**, 184 (2005), arXiv:nucl-ex/0410003 [nucl-ex].
- [3] K. Aamodt *et al.* (ALICE Collaboration), Phys. Rev. Lett. **105**, 252302 (2010), arXiv:1011.3914 [nucl-ex].
- [4] K. Aamodt *et al.* (ALICE Collaboration), Phys. Lett. **B708**, 249 (2012), arXiv:1109.2501 [nucl-ex].
- [5] S. Chatrchyan *et al.* (CMS Collaboration), JHEP **02**, 088 (2014), arXiv:1312.1845 [nucl-ex].
- [6] J. Adam *et al.* (ALICE Collaboration), Phys. Lett. **B B762**, 376 (2016), arXiv:1605.02035 [nucl-ex].
- [7] S. Mohapatra, *Measurement of the azimuthal anisotropy for charged particle production in Pb–Pb collisions at  $\sqrt{s_{NN}}=2.76$  TeV and in p–Pb collisions at  $\sqrt{s_{NN}}=5.02$  TeV with the ATLAS detector at the LHC*, Ph.D. thesis, SUNY, Stony Brook (2013-08-15).
- [8] A. Adare *et al.* (PHENIX Collaboration), Phys. Rev. Lett. **98**, 162301 (2007).
- [9] B. B. Abelev *et al.* (ALICE Collaboration), JHEP **06**, 190 (2015), arXiv:1405.4632 [nucl-ex].
- [10] J. Adam *et al.* (ALICE Collaboration), JHEP **09**, 164 (2016), arXiv:1606.06057 [nucl-ex].
- [11] G. Aad *et al.* (ATLAS Collaboration), Phys. Rev. **C86**, 014907 (2012), arXiv:1203.3087 [hep-ex].
- [12] S. Esumi (PHENIX Collaboration), *Proceedings, 11th International Workshop on Critical Point and Onset of Deconfinement (CPOD 2017): Stony Brook, NY, USA, August 7-11, 2017*, PoS **CPOD2017**, 018 (2018).
- [13] S. Acharya *et al.* (ALICE Collaboration), Eur. Phys. J. **C77**, 569 (2017), arXiv:1612.08975 [nucl-ex].
- [14] X. Zhu (ALICE), in *Proceedings, Workshop on Hadron Nuclear Physics (HNP 2013): Zhangjiajie, China, July 18-22, 2013* (2013) arXiv:1311.2394 [hep-ex].
- [15] B. B. Abelev *et al.* (ALICE Collaboration), Phys. Rev. **C90**, 054901 (2014), arXiv:1406.2474 [nucl-ex].
- [16] C. Bernardes (CMS Collaboration), *Proceedings, 2017 European Physical Society Conference on High Energy Physics (EPS-HEP 2017): Venice, Italy, July 5-12, 2017*, PoS **EPS-HEP2017**, 155 (2017).
- [17] A. M. Sirunyan *et al.* (CMS Collaboration), Phys. Rev. Lett. **121**, 082301 (2018), arXiv:1804.09767 [hep-ex].
- [18] C. Adler *et al.* (STAR Collaboration), Phys. Rev. Lett. **90**, 082302 (2003), arXiv:nucl-ex/0210033 [nucl-ex].
- [19] A. Adare *et al.* (PHENIX Collaboration), Phys. Rev. **C 77**, 011901 (2008).
- [20] S. Chatrchyan *et al.* (CMS Collaboration), Phys. Rev. **C84**, 024906 (2011), arXiv:1102.1957 [nucl-ex].
- [21] J. Adams *et al.* (STAR Collaboration), Phys. Rev. **C72**, 044902 (2005), arXiv:nucl-ex/0504031 [nucl-ex].
- [22] H. Agakishiev *et al.* (STAR Collaboration), Phys. Lett. **B704**, 467 (2011), arXiv:1106.4334 [nucl-ex].
- [23] S. Bass, P. Danielewicz, and S. Pratt, Phys.Rev.Lett. **85**, 2689 (2000), arXiv:0005044 [nucl-th].
- [24] S. Pratt, W. P. McCormack, and C. Ratti, Phys. Rev. **C 92**, 064905 (2015).
- [25] M. M. Aggarwal *et al.* (STAR Collaboration), Phys. Rev. **C82**, 024905 (2010), arXiv:1005.2307 [nucl-ex].
- [26] J. Adams *et al.* (STAR Collaboration), Phys. Rev. Lett. **90**, 172301 (2003), arXiv:nucl-ex/0301014 [nucl-ex].
- [27] B. Abelev *et al.* (ALICE Collaboration), Phys. Lett. **B723**, 267 (2013), arXiv:1301.3756 [nucl-ex].
- [28] S. Acharya *et al.* (ALICE Collaboration), “Two particle differential transverse momentum and number density correlations in p-Pb and Pb-Pb at the LHC,” (2018), arXiv:1805.04422 [nucl-ex].
- [29] S. Acharya *et al.* (ALICE Collaboration), Phys. Rev. Lett. **118**, 162302 (2017), arXiv:1702.02665 [nucl-ex].
- [30] M. Sharma and C. A. Pruneau, Phys. Rev. **C79**, 024905 (2009), arXiv:0810.0716 [nucl-ex].
- [31] T. Sjostrand, S. Mrenna, and P. Skands, JHEP **05**, 026 (2006), arXiv:0603175 [hep-ph].
- [32] G. Corcella, I. Knowles, G. Marchesini, S. Moretti, K. Odagiri, P. Richardson, M. Seymour, and B. Webber, JHEP **0101**, 010 (2001), arXiv:0011363 [hep-ph].
- [33] M. H. Seymour, AIP Conference Proceedings **357**, 568 (1996), <https://aip.scitation.org/doi/pdf/10.1063/1.49625>.
- [34] M. Estienne, Phys.Atom.Nucl. **71**, 1535 (2008), arXiv:0810.1698 [nucl-ex].
- [35] B. Abelev *et al.* (ALICE Collaboration), Phys. Rev. **D91**, 112012 (2015).
- [36] C. Pruneau, S. Gavin, and S. Voloshin, Phys. Rev. **C66**, 044904 (2002), arXiv:0204011 [nucl-ex].
- [37] P. Z. Skands, Phys. Rev. **D82**, 074018 (2010), arXiv:1005.3457 [hep-ph].
- [38] T. Sjostrand and P. Skands, Eur. Phys. J. **C39**, 129 (2005), arXiv:0408302 [hep-ph].
- [39] M. Sandhoff and P. Skands, in *Physics at TeV colliders. Proceedings, Workshop, Les Houches, France, May 2-20, 2005*, 234 (2006) arXiv:hep-ph/0604120 [hep-ph].
- [40] A. Buckley, H. Hoeth, H. Lacker, H. Schulz, and J. E. V. Seggern, Eur. Phys. J. **C65**, 331 (2010), arXiv:0907.2973 [hep-ph].
- [41] B. Andersson, G. Gustafson, G. Ingelman, and T. Sjostrand, Phys. Rept. **97**, 31 (1983).
- [42] J. Pumplin, D. Stump, J. Huston, H. Lai, P. Nadolsky, and W. Tung, JHEP **0207**, 012 (2002), arXiv:0201195 [hep-ph].
- [43] H. L. Lai, J. Huston, S. Kuhlmann, a. Morfin, F. Olness, J. F. Owens, J. Pumplin, and W. K. Tung, Eur. Phys. J. **C12**, 375 (2000), arXiv:9903282 [hep-ph].

- [44] A. Mueller and W.-K. Tang, Phys. Lett. **B**, 123 (1992).
- [45] G. P. Salam, Acta Phys.Polon. **B30**, 27 (1999), arXiv:9910492 [hep-ph].
- [46] A. C. Diaz, G. C. Balbastre, and C. G. Trápaga, <http://scielo.sld.cu/pdf/nuc/n50/nuc035011.pdf> (2011).
- [47] P. Csizmadia, P. Lévai, S. E. Vance, T. S. Biró, M. Gyulassy, and J. Zimányi, Journal of Physics G: Nuclear and Particle Physics **25**, 321 (1999).
- [48] D. Molnar and S. A. Voloshin, Phys. Rev. Lett. **91**, 092301 (2003), arXiv:nucl-th/0302014 [nucl-th].
- [49] J. Adams *et al.* (STAR), Phys. Rev. **C75**, 034901 (2007).
- [50] B. I. Abelev *et al.* (STAR Collaboration), Phys. Rev. **C80**, 064912 (2009), arXiv:0909.0191 [nucl-ex].
- [51] A. Adare *et al.* (PHENIX Collaboration), Phys. Rev. **C78**, 014901 (2008), arXiv:0801.4545 [nucl-ex].
- [52] Y. K. Kim *et al.*, Phys.Rev.Lett. **63**, 1772 (1989).
- [53] M. Tanabashi *et al.* (Particle Data Group), Phys. Rev. D **98**, 030001 (2018).